Widely Tunable Morphologies in Block Copolymer Thin Films Through Solvent Vapor Annealing Using Mixtures of Selective Solvents

*Michelle A. Chavis, Detlef-M. Smilgies, Ulrich B. Wiesner, and Christopher K. Ober**

Thin films of block copolymers are extremely attractive for nanofabrication because of their ability to form uniform and periodic nanoscale structures by microphase separation. One shortcoming of this approach is that to date the design of a desired equilibrium structure requires synthesis of a block copolymer de novo within the corresponding volume ratio of the blocks. In this work, solvent vapor annealing in supported thin films of poly(2-hydroxyethyl methacrylate)-*block*-poly(methyl methacrylate) [PHEMA-*b*-PMMA] by means of grazing incidence small angle X-ray scattering (GISAXS) is investigated. A spin-coated thin film of a lamellar block copolymer is solvent vapor annealed to induce microphase separation and improve the long-range order of the self-assembled pattern. Annealing in a mixture of solvent vapors using a controlled volume ratio of solvents, which are chosen to be preferential for each block, enables selective formation of ordered lamellae, gyroid, hexagonal, or spherical morphologies from a single-block copolymer with a fixed volume fraction. The selected microstructure is then kinetically trapped in the dry film by rapid drying. This paper describes what is thought to be the first reported case where in situ methods are used to study the transition of block copolymer films from one initial disordered morphology to four different ordered morphologies, covering much of the theoretical diblock copolymer phase diagram.

1. Introduction

Bottom-up patterning techniques using the inherent self-assembly properties of nanometer length scale materials have drawn great interest as an alternative or companion to traditional top-down lithography techniques. Among these alternative systems, block copolymers (BCPs) are attractive because of their ability to phase separate into various well-defined morphologies with length scales ranging from 10 to 100 nm. There are numerous nanotechnology applications that are enabled because of advances made in materials and their ability to self-assemble into well-defined ordered structures. Fields, such as microelectronics, solar energy devices, energy storage materials, and a plethora of other applications, have benefited from these advances.[1,2] However, obtaining a specific morphology normally requires synthesis of a block copolymer de novo. Thus having the ability to precisely and reproducibly fine-tune the morphology of a given block copolymer by a simple solvent vapor treatment is of great interest and will facilitate further advances in nanotechnology applications.

For example, typically to obtain block copolymer patterns with different morphologies, one would have to synthesize a series of block copolymers with the specific volume ratios for each block that lies within the appropriate composition range of the phase diagram.[3] Being able to precisely select a specific block copolymer morphology through synthesis alone is challenging and sometimes difficult to achieve, particularly in the case of the co-continuous cubic gyroid phase, which only occurs within a narrow range of compositions.[4–6]

Block copolymer thin films with well-defined thickness and small surface roughness are typically deposited with spin coating. The fast drying time in spin coating often leaves the block copolymer film in a kinetically frozen state with only a short-range order. Traditionally, thermal annealing has been used as an effective technique for improving nanostructure domains and annealing defects, thus increasing the ordered grain size; however, in many materials, the high temperature and long annealing times can be detrimental and can lead to the degradation of one or both blocks. Solvent vapor annealing (SVA) has proven to be an effective alternative.[7–10] Recently, it has also been found that SVA provides avenues to structures that are unattainable through thermal annealing.[6,10–14]

Through solvent vapor annealing with selective and nonselective solvents, it has previously been shown to be possible to obtain up to two different block copolymer morphologies starting with the same material. Bosworth and co-workers demonstrated that by solvent annealing poly(α-methylstyrene)-*block*-poly(4-hydroxystyrene) (PαMS-*b*-PHOST) in two different

Dr. M. A. Chavis, Prof. U. B. Wiesner, Prof. C. K. Ober
Department of Materials Science and Engineering
214 Bard Hall
Cornell University
Ithaca, NY 14853, USA
E-mail: cko3@cornell.edu
Dr. D.-M. Smilgies
Cornell High Energy Synchrotron Source
161 Synchrotron Drive
Cornell University
Ithaca, NY 14853, USA

DOI: 10.1002/adfm.201404053

solvents, either tetrahydrofuran (THF) or acetone, it is possible to obtain either the cylindrical or spherical morphologies at high swelling ratios, respectively;[6,13] structures could be quenched by rapid drying, with some associated contraction in the perpendicular direction. It was also shown that switching between the two dry states via the appropriate solvent vapor annealing cycle was possible.[6] Bosworth et al.[11,15] then went on to show that it is possible to lock two morphologies on one surface with the use of electron beam irradiation.

Ross and co-workers[16] followed this line of work using poly(styrene)-*block*-poly(dimethylsiloxane) (PS-*b*-PDMS) as the polymer, and acetone (cylindrical patterns) or dimethylformamide (spherical patterns) as the solvents. Jeong et al.[17] used poly(2-vinylpyridine)-*block*-poly(dimethylsiloxane) (P2VP-*b*-PDMS) and with numerous solvents (isopropyl alcohol, ethanol, methanol, pentanol, acetic acid, pyridine, etc.) were able to achieve the spherical, cylindrical, perforated lamellae and lamellar morphologies. It is important to note that in this system, the surface was treated with a PDMS homopolymer before the diblock copolymer was deposited, and post etching was necessary to reveal the structure. Jung and co-workers, as well as Gotrik and co-workers, then used a mixture of solvents (toluene and *n*-heptane) to vapor anneal films of PS-*b*-PDMS to achieve lamellae, perforated lamellae, and cylindrical patterns. Again, the surface was treated before the deposition and annealing of the diblock copolymer and etching was required to reveal the structures, and the final morphology was film thickness dependent.[12,17] In more recent work, PS-*b*-PDMS with a starting synthesized double-gyroid morphology in the bulk was able to form spheres, cylinders, and perforated lamellae in thin films through solvent annealing relying heavily on the film thickness and microdomain period,[18] a result that was also found by She et al.[19] for the poly(styrene)-*b*-poly(L-lactic acid) system.

In this work, a systematic method to precisely select one of four different and specific block copolymer morphologies from a single-block copolymer is investigated; this selectivity is achieved by controlling just the solvent vapor annealing conditions, specifically the mixing ratios of selective solvents for each block, and the amount of time permitted for the annealing process to take place. The phase selection behavior in supported thin films of poly(2-hydroxyethyl methacrylate)-*block*-poly(methyl methacrylate) (PHEMA-*b*-PMMA) was then explored in situ and in real time using grazing-incidence small-angle X-ray scattering (GISAXS) and optical film thickness monitoring.

2. Results and Discussion

Annealing of the as-spun samples in the vapor of different volume/volume ratios of methanol (MeOH) and tetrahydrofuran (THF) solvent mixtures allows for precise control and predictability of the resulting block copolymer morphology. By choosing the correct volume/volume ratios of the solvents, we are able to explore the phase diagram for diblock copolymers using just one block copolymer.

A combination of complementary techniques was applied to characterize film topography and surface morphology. Grazing incidence small-angle X-ray scattering (GISAXS) and small-angle X-ray scattering (SAXS) were used to determine and identify the ordered state symmetries in thin films and polymer bulk, respectively, over macroscopic probing areas/volumes (GISAXS: 0.5 mm × 20 mm; SAXS: 0.5 mm × 0.5 mm × 0.5 mm). GISAXS was used to probe the film interior and provide an accurate representation of the morphology throughout the entire film.[8,20] All GISAXS images were taken at incident angles that varied between 0.10° and 0.20°, angles that are slightly higher and lower than the critical angles of the polymer film and silicon substrate, respectively. Scattering experiments were conducted at the Cornell High Energy Synchrotron source (CHESS) at station G1.

The block copolymer used in this study, PHEMA-*b*-PMMA, was synthesized via anionic polymerization with total molecular weight of 40K, and nominally equal block volume fractions with a dispersity ($Đ$) of 1.08, resulting in an equilibrium lamellar morphology. This block copolymer was chosen because of its combination of polar and nonpolar blocks. With appropriate chemistries and photoactive compounds, it has the ability to behave both as a traditional top-down photoresist and a self-assembling block copolymer.

2.1. Bulk PHEMA-*Block*-PMMA Results

First, it was important to verify the morphology of the starting bulk diblock copolymer. Bulk PHEMA-*b*-PMMA (polymer structure, **Figure 1**a) with equal volume fractions was stirred and dissolved in 2-methoxyethanol (2-MOE) for 24 h. 2-MOE is a good nonselective solvent for both blocks of the BCP, and thus we expect the block copolymer to retain its equilibrium morphology.[22] Upon complete dissolution, the polymer solution was cast into a PTFE dish at 50 °C covered with a glass hemisphere to let the solvent evaporate slowly. A drying temperature of 50 °C is well below the glass transition temperatures of both blocks (T_g(PHEMA) = 118 °C; T_g(PMMA) = 105 °C)[23] and does not provide polymer mobility for self-assembly of the polymer to occur after solvent evaporation. Films were, therefore, subsequently placed in a vacuum oven at 180 °C for 3 d to degas and self-assemble into their equilibrium morphology.

Figure 1b,c shows SAXS and TEM results, respectively, of the pristine polymer after it has been annealed. The PHEMA-*b*-PMMA copolymer was stained using phosphotungstic acid. Staining resulted in the PHEMA block being darker than the PMMA block. From the data we can conclude that the polymer exhibits a lamellar morphology. The SAXS pattern of this polymer is consistent with the lamellar morphology, exhibiting characteristic peaks with ratios of $q/q^* = \sqrt{1}, \sqrt{4}$, and $\sqrt{9}$ (Figure 1c), where q denotes the length of the scattering vector and q^* denotes the position of the first diffraction peak. The observation of the even-order $\sqrt{4}$ peak suggests that the lamellar structure was asymmetric. The lattice spacing as measured by SAXS was 41.8 nm, consistent with the estimated 40 nm spacing from transmission electron microscopy (TEM). This confirms that the equilibrium morphology of the PHEMA-*b*-PMMA block copolymer is indeed lamellar.

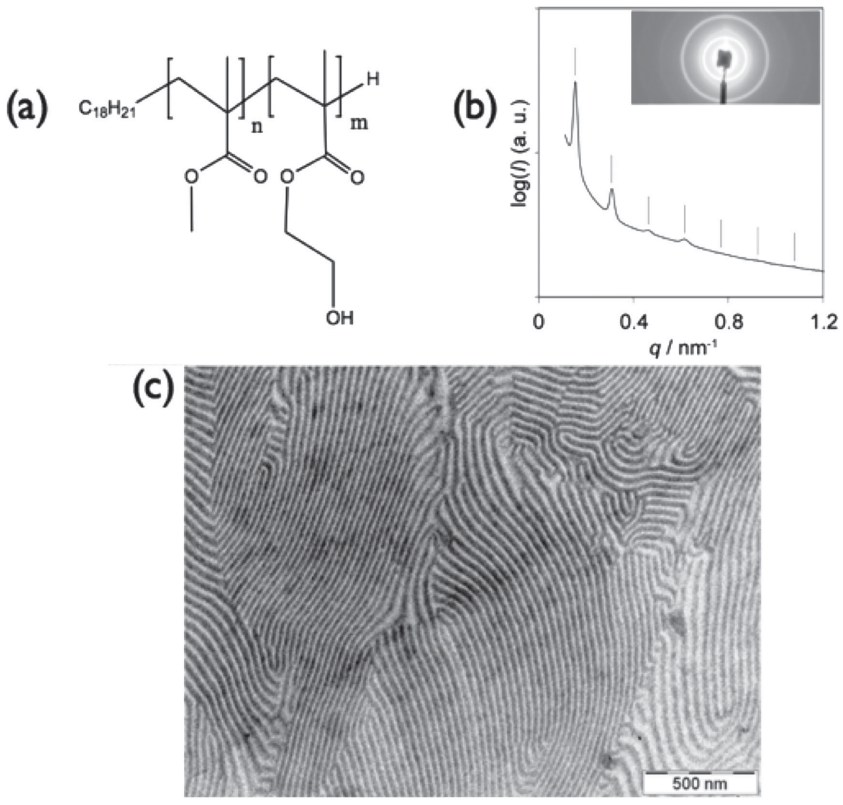

Figure 1. a) Chemical structure of di-block copolymer PHEMA-*b*-PMMA. b) SAXS of thermally annealed PHEMA-*b*-PMMA film. c) Transmission electron microscopy image of stained PHEMA-*b*-PMMA.

2.2. Choice of Solvents for Vapor Annealing

The microphase separation of diblock copolymers is governed by the segregation strength, χN, which is the product of the Flory–Huggins interaction parameter, χ, and the degree of polymerization, N, defined as the number of monomer units in the polymer.[1,24] The affinity of a solvent for a certain block is governed by the particular solvent–polymer interaction parameter, χ_{ps}.[23] The χ_{ps} parameter is proportional to the chemical incompatibility between the block and the solvent. Similarly, χ_{AB} is proportional to the chemical incompatibility of blocks A and B. This parameter also governs behavior such as the order–disorder transition temperature, microstructure, and periodicity, all of which are important in self-assembly.

The Hildebrand solubility parameter, δ, defined as the square root of the cohesive energy, is a good way to estimate the degree of interaction between two species, for example a polymer and a solvent. Materials with similar δ values are more likely to be miscible with each other. The solubility parameters of PHEMA, PMMA, THF, and MeOH are 26.93 $(MPa)^{1/2}$, 18.6–26.4 $(MPa)^{1/2}$, 18.6 $(MPa)^{1/2}$, and 29.63 $(MPa)^{1/2}$, respectively.[23] Based on these δ values, methanol is a good solvent for PHEMA whereas it is not a good solvent for PMMA, and THF is a good solvent for PMMA and not a good solvent for PHEMA.[23] As demonstrated below, by choosing selective solvents for each block, and controlling the volume/volume ratios of each solvent mixture, we were able to control the swelling of each block and hence control and direct the block copolymer toward a specific desired morphology. The Hildebrand solubility parameter can be used to estimate the χ parameter between a polymer and a solvent, χ_{ps}, using[1]

$$\chi_{ps} = 0.34 + V_s / RT\left(\delta_s - \delta_p\right)^2 \quad (1)$$

χ consists of two components, the enthalpic and entropic parts. The enthalpic part is expressed in terms of the Hildebrand solubility parameters. Calculations for χ_{ps}, χ_{AB}, and χN for the specific block copolymer and solvents used in this study are shown in **Table 1**. The high χN value indicates that the dry block copolymer is in the strong segregation regime.

The solvent mixture of THF and MeOH has other advantageous properties as well; the vapor pressures, as well as melting and boiling points of both liquids, are well matched. Hence, the concentration of one component is not bound to diminish over time due to faster evaporation. Indeed, the vapor–liquid equilibrium of THF and MeOH closely follows Raoult's law for ideal solutions.[25] In the following discussion, it is assumed that the vapor concentrations and the partial pressures in the vapor closely follow the volume ratios of the liquid mixture.

In polymer–solvent systems, the thermodynamic control parameter is the polymer content, f, in the solution.[9,26] In our study, a spectroscopic reflectometer (FilMetrics) was used as a film thickness monitor. Following Krausch and co-workers,[9,27] we can assume that when the polymer film swells in the vapor, it remains laterally constrained so that it will essentially swell by increasing its thickness. In this case, the swelling ratio, f, is simply determined by the ratio of swollen film thickness, d, over dry polymer film thickness, d_0,

$$f = d / d_0 \quad (2)$$

Hence, our system is characterized by the volume fraction, ϕ, of the PHEMA block of the PHEMA-*b*-PMMA diblock copolymer, the THF concentration, x, in the liquid mixture, and the polymer fraction, f (in%).

Table 1. Calculations of different χ values.

χ interactions	Calculated interactions
$\chi_{PMMA\text{-}THF}$	0.3403
$\chi_{PMMA\text{-}MeOH}$	2.3523
$\chi_{PHEMA\text{-}THF}$	2.6666
$\chi_{PHEMA\text{-}MeOH}$	0.4653
$\chi_{PHEMA\text{-}PMMA}$	0.3589
χN	126.86

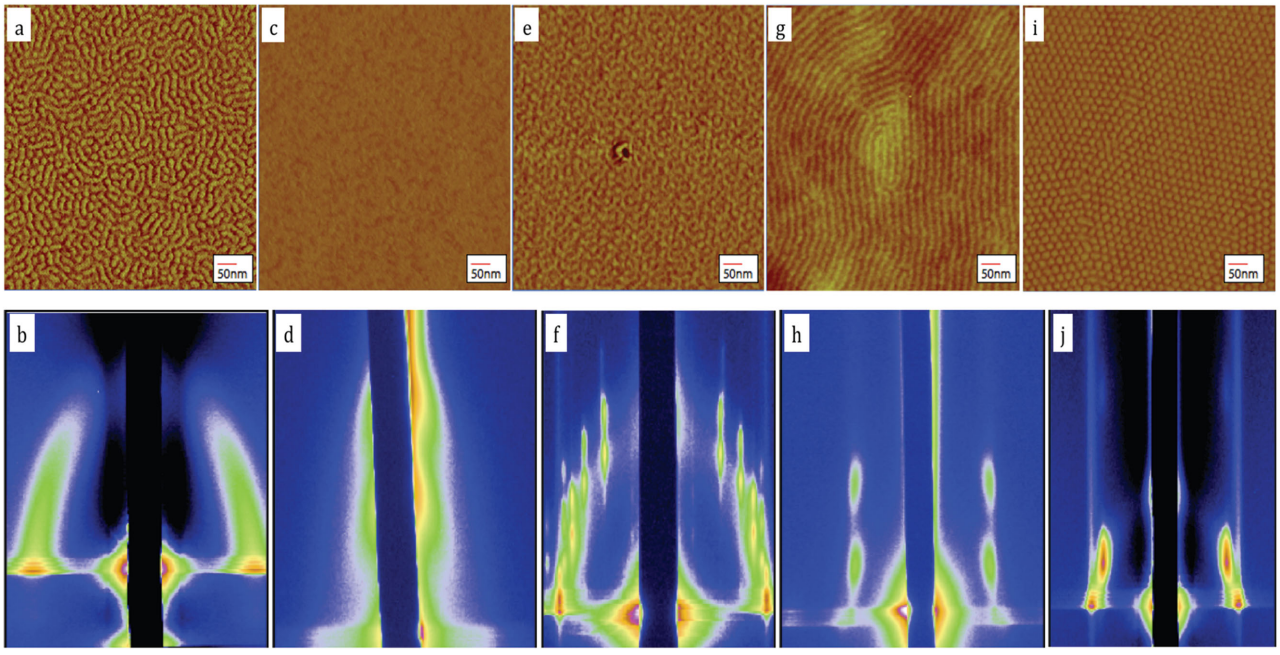

Figure 2. AFM and GISAXS results for PHEMA-*b*-PMMA films from different solvent annealing treatments and after subsequent film drying. a,b) As-spun, no anneal; c,d) annealed for 45 min in 80/20 v/v THF/MeOH; e,f) annealed for 45 min in 50/50 v/v, THF/MeOH; g,h) annealed for 45 min in 20/80 v/v THF/MeOH; i,j) annealed for 3–4 h in 50/50 v/v THF/MeOH.

In the following, we are studying a polymer with ϕ close to 0.5 in the lamellar phase. All experiments were undertaken under ambient conditions, $T = 25$ °C and $p = 1$ atm. **Figure 2** shows the volume/volume compositions of the solvents needed to obtain the various morphologies along with accompanying AFM and GISAXS images after solvent annealing. A detailed insight into the mechanism of morphology formation was obtained by performing an in situ GISAXS study during solvent vapor annealing. Using GISAXS to probe the interior of the film during the annealing process in combination with a thickness monitor allows for establishing correlations between solvent mixtures, swelling ratio, annealing time, and corresponding morphology. For example, Bosworth et al.[11] and Paik et al.[6] both used in situ methods for studying the transition between different block copolymer film morphologies cycling through the spherical to cylindrical microstructures.

Thin films were prepared by spin-coating (1650 rpm; 65 s) films of the PHEMA-*b*-PMMA copolymer in ethyl lactate (5% w/v) onto a native oxide silicon wafer (30 mm × 30 mm) to a dry film thickness of 145–150 nm. The fast evaporation of the ethyl lactate solvent provided insufficient time for long-range ordering of the block copolymer as evidenced by the atomic force microscopy image of the as-cast film. Next, the as-cast films were exposed to a mixture of MeOH and THF as the annealing solvents for the block copolymer at room temperature. This liquid mixture was injected into the annealing chamber with a controlled nitrogen counter-flow used to manage the degree of swelling of the polymer film. After annealing for specific times as described in **Table 2**, the films were rapidly dried by removing them from the annealing vessel as quickly as possible and by allowing the solvent vapors to fully evaporate from the film. GISAXS confirmed that no morphology changes took place once the films were dried indicating that the microdomain structures obtained during vapor annealing were well preserved, despite the pronounced shrinkage of the films during rapid drying.[6,15]

2.3. Solvent Vapor Annealing of PHEMA-*Block*-PMMA Thin Films

Mixed solvent vapor annealing of PHEMA-*b*-PMMA films in various volume/volume ratios of THF and MeOH enabled a "walk through" of the universal block copolymer phase diagram obtaining ordered lamellar, gyroid, hexagonal, and spherical morphologies.[1] It is believed that reordering occurs due to the increased mobility that the solvent vapor provides to the individual polymer chains.[20,28] In the following, we will individually discuss the morphologies obtained with different vapor mixtures.

2.3.1. As-Spun Film

Figure 2a,b shows the AFM image and GISAXS profile, respectively, of the as-spun film. The GISAXS image exhibits a partial powder ring that is associated with block copolymer phase separation, but only shows the first-order scattering, indicating that no long-range order was formed. Combining AFM and GISAXS results we concluded that as-spun films formed a metastable structure of vertical lamellae with an only short-range order. Indexing the structure, it is shown to have a period of 29 nm (Figure S1, Supporting Information). Such vertical structures can be formed due to the rapid solvent evaporation, which are typically metastable.[20,29]

Table 2. Solvent mixtures and times leading to various morphologies and the structural morphology in the dry phase after solvent vapor annealing. Lattice constant firs are good to about ±2 nm.

Solvent Vol/Vol mixtures (THF/MeOH)	Swell time [s]	Final resulting morphology	Polymer volume fraction (f)	Lattice parameter [nm]	Vertical shrinkage [%]
As-Cast	n.a.	Perpendicular lamellae	100%	29	n.a
80/20 (swollen state)	6300	Parallel lamellae, swollen	32%	32	None
80/20 (dry state)	n.a.	Parallel lamellae, dry	100%	15	50%[a)]
50/50 (swollen state)	6300	BCC (110) spheres, swollen	40%	42	None
50/50 (dry state)	n.a.	BCC (110) spheres, dry	100%	42	42%
20/80 (swollen state)	6300	Parallel cylinders swollen	33%	35	None
20/80 (dry state)	n.a.	Parallel cylinders dry	100%	35	35%
50/50 (swollen state)	20 700	(Hexagonal)[b)]	40%		
50/50 (dry state)	n.a.	Gyroid (211) dry	100%	71	45%

n.a.: not applicable; [a)]Estimated from lamellar periods; [b)]Structure was not identified.

2.3.2. Annealing in a Vapor of an 80/20 (v/v) Mixture of THF/MeOH

Figure 2c,d shows the AFM and GISAXS results, respectively, of an as-spun film that has been annealed in the vapor of an 80/20 (v/v) THF/MeOH solvent mixture. Upon injection of the mixed solvent, the partial powder ring gradually changed from predominantly perpendicular lamellae to parallel lamellae (Figure S2, Supporting Information). The film was swollen for 45 min and reached a final swollen film thickness of 460 nm, i.e., swelling more than 300% relative to its original film thickness, which corresponds to a polymer volume fraction of 32%. The GISAXS images of the fully swollen film (Figure S3, Supporting Information) revealed a peak behind the beamstop. After quenching, the GISAXS image of the dried film displayed two ellipsoidal shaped peaks behind the beam stop. For the fully swollen film, the peaks were sharp and intense; however, the quenched film shows broad peaks behind the beam stop (Figure 2d). In both images, there are no other peaks in the Yoneda band or elsewhere. Such a scattering pattern is expected for lamellae oriented parallel to the substrate.[20] The incident angle was chosen below the critical angle of the substrate, and the (001) peak associated with the scattering of the reflected beam is seen in Figure 2d in addition to the regular reflection of the direct beam ("double vision"). [20] The AFM image (Figure 2c) shows a featureless and flat image, which is what is expected of lamellar domains parallel to the substrate and in agreement with the GISAXS image.[20]

In the course of swelling, the lamellar period was determined to be 32 nm for both parallel and perpendicular lamellae (see Figure S2 in Supporting Information), which is somewhat larger than the lamellar period of the as-cast film of 29 nm, whereas the dried film displayed a reduced lamellar period of 15 nm, indicating a significant, drying-induced shrinkage of the lamellar stack. Our observations are consistent with the in-depth studies by Papadakis and co-workers on vertical lamellae[30]. Similarly, Gu et al.[13] observed an initial lattice expansion during vapor treatment in thin films in the hexagonal cylinders phase. The strong reduction in lamellar period after rapid drying appears to be similar to the findings of Jeong et al.[17] after processing.

2.3.3. Annealing in a Vapor of a 20/80 (v/v) Mixture of THF/MeOH

Figure 2g,h shows the AFM and GISAXS results, respectively, obtained of an as-spun film that has been annealed in the vapor of a 20/80 (v/v) ratio of the THF/MeOH solvent mixture. After solvent injection, the scattering of the as-cast film disappeared completely leaving a featureless scan. The film was swollen for 45 min and reached a final thickness of 440 nm, corresponding to a similar polymer fraction of $f = 33\%$, which is comparative to the lamellae forming 80/20 (v/v) (THF/MeOH) film. The GISAXS image of the fully swollen film (Figure S5, Supporting Information) revealed peaks that are sharp and intense consistent with a parallel cylinder morphology with a hexagonal lattice constant of 35 nm. The film was then quenched quickly to lock in the achieved order. The indexing of the subsequent GISAXS image of the fully dried film (Figure 2h) revealed a uniaxial contraction had occurred along the surface normal and an associated shift in the q_z peak positions. The in-plane lattice constant remained at 35 nm; however, the lattice had to be shrunk to 35% vertically, i.e., drying induced a significant distortion of the cubic lattice. The shrinking ratio compares well with the shrinkage of the film thickness back to 150 nm after drying. The AFM image (Figure 2g) shows a fingerprint pattern, which is expected of lying cylinders and is in agreement with the interpretation of the GISAXS results.

2.3.4. Annealing in a Vapor of a 50/50 (v/v) Mixture of THF/MeOH

After establishing that the thin-film morphology could be changed from the equilibrium lamellar morphology (80/20 THF/MeOH v/v mixture) to a cylinder morphology (20/80 THF/MeOH v/v mixture), our next goal was to achieve the remaining spherical and gyroid phases with an intermediate vapor mixture. Figure 2i,j shows the AFM and GISAXS results, respectively, of an as-spun film that has been annealed in the vapor of a 50/50 (v/v) THF/MeOH solvent mixture. Once again, after injection of the solvent the GISAXS scattering pattern became featureless, an indication of massive reorganization

of the polymer chains (data not shown). At a film thickness of 368 nm, corresponding to a polymer volume fraction of 40%, the characteristics peaks of the GISAXS pattern were those of the spherical morphology beginning to form. The associated BCC packing of the spheres of the minority block had a cubic lattice constant of 42 nm. (Figure S7, Supporting Information). The transformation from the cylinder phase to the spherical phase was shown in an earlier study;[6,11] however, in that case, the starting morphology was the cylinder phase.

The film was again held under these annealing conditions for 45 min and then quenched quickly to lock in the achieved morphology. The GISAXS pattern of the quenched film (Figure 2j) can be indexed by a bcc lattice with its (110) face parallel to the substrate and a lattice constant of 42 nm, if a 42% vertical contraction of the film is taken into account. As in the case of the parallel cylinders, the vertical shrinkage is close to the overall change in film thickness. The AFM image (Figure 2i) shows dots forming a centered rectangular pattern, which is what is expected of either a spherical morphology or standing cylinders. Using the GISAXS scan, it can be concluded that the assignment to a spherical morphology is the correct one.

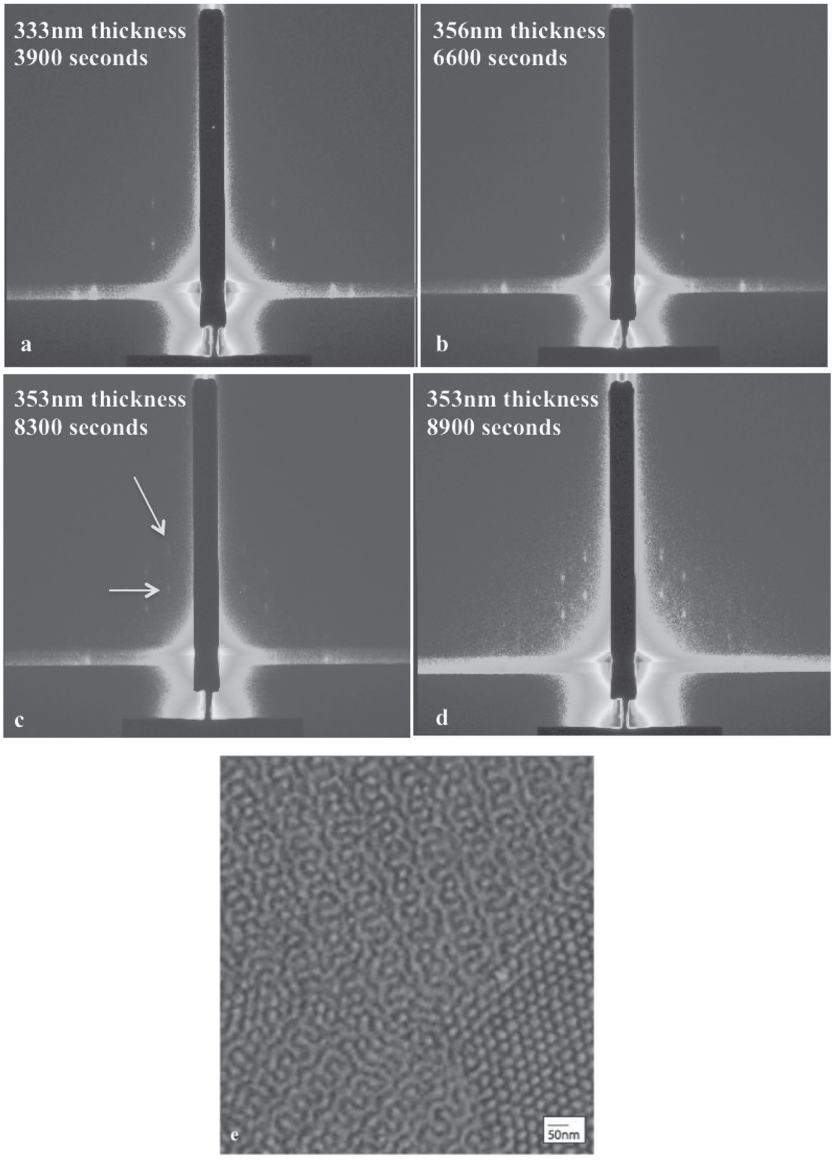

Figure 3. a–d) Time lapsed GISAXS of spherical to gyroid morphology transition. e) AFM showing the coexistence of gyroid and spherical morphology.

2.3.5. Long-Term Annealing in Vapor of a 50/50 (v/v) Mixture of THF/MeOH

Annealing of a film for 45 min in a 50/50 (v/v) mixture of THF/MeOH yielded a spherical morphology (vide supra). In contrast, when this same film was annealed for a longer time (≈3–4 h) the peaks became stronger and sharper whereas the swollen thickness of the film remained at 353 nm. Gradually, during further annealing in the swollen state, other peaks started to appear (Figure 3). While we were unable to obtain a satisfactory fit of the GISAXS pattern, the peak pattern had the appearance of a hexagonal structure. Upon fast drying of the film the subsequent GISAXS experimental results were consistent with a gyroid morphology.[4,10,19,31] The GISAXS pattern (Figure 2f) can be indexed with the 022, 202, 121, 21–1, 2–1–1 reflections of the scattered and direct reflected beams. The gyroid structure has the (211) plane parallel to the substrate.[4,31] Consistent with the other quenched films this film also showed strong shrinkage of ≈45% compared with the ideal cubic gyroid morphology. This shrinkage can again be attributed to the rapid drying and has been observed before in various other studies of BCPs under solvent vapor annealing.[4,10,19,31] Figure 2e shows the corresponding AFM image of the thin film and the observed characteristic pinwheel pattern of the gyroid agrees with the interpretation of the GISAXS results.

The transformation from the spherical to gyroid phase was further investigated with the same in situ methods discussed above. To our knowledge, this is the first reported case where a transition is observed from the spherical to the gyroid phase in thin films of a linear diblock copolymer. As the initially formed spherical phase seemed to slowly transform into the gyroid phase, it can be speculated whether the spherical phase is a metastable phase that forms when the original lamellae rearrange to form the thermodynamically stable gyroid phase. As the break-up of the lamellar phase and the formation of the bicontinuous gyroid phase involve a large amount of mass transport, it is conceivable that the intermediate spherical phase formed as a step along the path.

Figure 3 shows the in situ GISAXS patterns at different time points during the transition from the spherical to the gyroid morphology. The polymer film reaches a thickness of 368 nm and

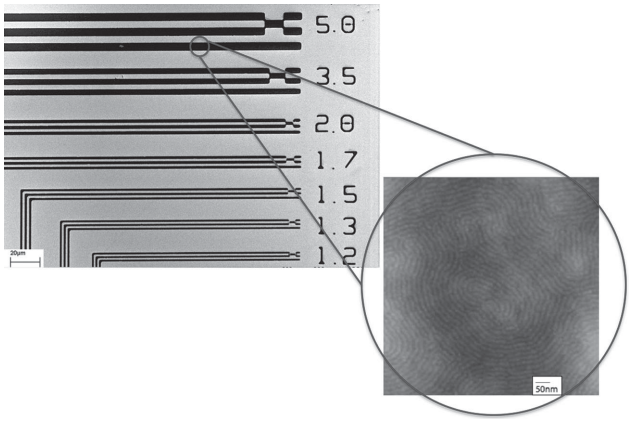

Figure 4. Scanning electron microscopy image of photolithographically patterned PHEMA-*b*-PMMA with discernible lines down to 1.2 µm. The insert shows the polymer's ability to phase separate via solvent vapor annealing in the patterned lines.

was allowed to sit at this thickness for several hours. At 3900 s, peaks appeared that clearly identify the structure as spherical (Figure 3a). As this same film is allowed to sit longer, see time points at 6600 s (Figure 3c) and 8900 s (Figure 3d), we can see the evolution of peaks consistent with the transition from the spherical morphology to another morphology. This second intermediate structure has the appearance of distorted hexagonal cylinders and does not seem to be related to the gyroid morphology (Figure S9, Supporting Information). Figure 3e shows an AFM image of the PHEMA-*b*-PMMA thin film that was solvent vapor annealed in a 50/50 (v/v) mixture of THF/MeOH and quenched at the 8300 s mark. From this image, we can clearly see a coexistence of domains with spherical and gyroid morphology in the same film that could be an effect of the slow kinetics of the transformation observed in the in situ study.

2.3.6. Demonstration of Lithography Capability with Hierarchical Patterning

As a proof-of-principal experiment, we tested the block copolymer's ability to act as both a photoresist patternable by DUV exposure and to simultaneously form patterned structures using directed self-assembly. A mixture of 4% tetramethoxymethylglycoluril (TMMGU, Powderlink 1174, Cytec Industries) and 1.5% triphenylsulfonium triflate (TPST) relative to the amount of block copolymer was added to a solution of PMMA-*b*-PHEMA in ethyl lactate to provide required chemistries needed for the BCP to behave as a photoresist. The PHEMA block was carefully chosen for this purpose as its functionality enables the block to behave as a negative-tone photoresist with the addition of a photoacid generator (TPST) and crosslinker (TMMGU) and still retain its self-assembly properties. This cross-linking chemistry is well known and has been used by us with other block copolymers.[32] The polymer solution (2% w/v) was spin-coated (1650 rpm; 65 s) onto a native oxide silicon wafer (30 mm × 30 mm) to a thickness of 53 nm from ethyl lactate. Next, the film was exposed to a 254 nm UV light source for photopatterning using a mask aligner (ABM Contact Aligner). The UV exposure was followed by a post-exposure bake for 60 s at 115 °C followed by a development step for 5 min in THF. **Figure 4** shows results of scanning electron microscopy (SEM) demonstrating the ability of the PMMA-*b*-PHEMA copolymer to be useful for "top-down" photolithography patterning techniques. The SEM image shows patterns with resolution down to the 1.2 µm scale. This resolution is consistent with the use of a mask aligner. A higher resolution would be expected by the use of a more sophisticated top-down lithography patterning tool.

3. Conclusions

The ability to have control and predictability of block copolymer domains and nanostructures and to selectively form complex microstructures from simple block copolymer morphologies will be essential for applications that increasingly depend on directed self-assembly. Solvent vapor annealing is a powerful technique that allows for direct tuning to a specific morphology. We have shown the ability to target a specific morphology of self-assembled domains of PHEMA-*block*-PMMA through selective solvent vapor annealing. Not only have we demonstrated the ability to move with ease through the phase diagram with one block copolymer by changing the volume compositions of the paired solvents used for annealing, we have also shown for the first time a transition from the spherical to gyroid morphology. We have shown that a treatment of block copolymer thin films with a mix of selective solvents and successive rapid drying can be used to obtain four different block copolymer morphologies from the same initial polymer. An overview is provided in Table 2. Our real-time in situ study has revealed pathways of the solvent vapor annealing process of the polymer. We further show that there is a very slow kinetics involved with the transformation of the unexpected spherical phase to the gyroid phase. Finally, we demonstrate that the used polymer is compatible with lithography, which potentially opens up a path to obtain well-controlled, locked-in hierarchical nanostructures in thin film form.

4. Experimental Section

Materials: Poly(2-hydroxyethyl methacrylate)-*block*-poly (methyl methacrylate), PHEMA-*b*-PMMA with $M_{n,PHEMA}$ = 20 kg mol^{-1}, $M_{n,PMMA}$ = 20 kg mol^{-1} and PDI = 1.04 was synthesized by sequential anionic polymerization, as described elsewhere.[33] Methanol (MeOH), tetrahydrofuran (THF), and ethyl lactate (EL) were purchased from Fisher Scientific. Nitrogen gas was purchased from Airgas. All purchased materials were used as received.

Thin Film Sample Preparation: PHEMA-*b*-PMMA was first dissolved in EL to form a 5% (w/v) stock solution and allowed to stir for 24 h to ensure a well-mixed solution. Thin films were prepared by spin-coating the solution at 1650 rpm for 65 s onto native oxide silicon wafer pieces 2 cm × 2 cm in size. Sample thickness ranged from 145 to 155 nm and was measured using a Filmetrics F20 spectroscopic reflectometer.

Solvent Annealing: The solvent annealing chamber is a custom-made vapor cell with an integrated film thickness monitor (**Scheme 1**).[6] The cell has inlets for liquid solvent, as well as for a gas flow. For solvent annealing, samples were placed inside the solvent annealing chamber on the sample stage. A controlled, counter flow of nitrogen gas was introduced inside the solvent annealing chamber. The nitrogen gas

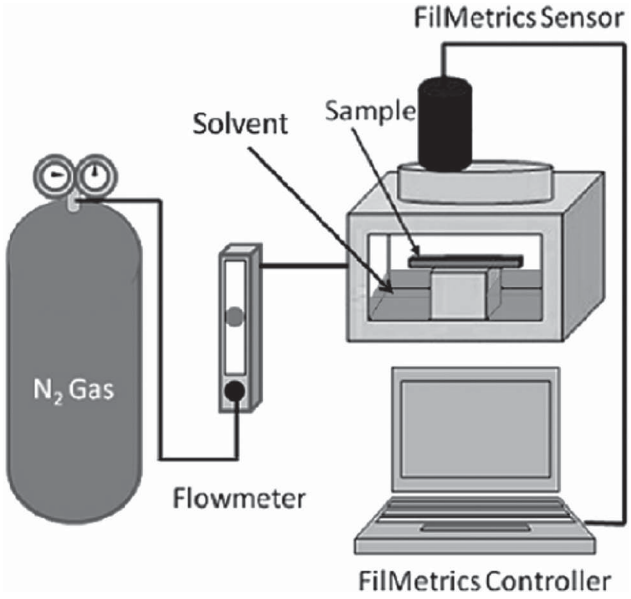

Scheme 1. Experimental setup of the in situ solvent vapor processing chamber. Reproduced with permission.[6] Copyright 2010, American Chemical Society.

was controlled using a Cole-Palmer aluminum flowmeter with a high-resolution valve (143 sccm maximum flow for nitrogen). This nitrogen counter flow provides a precise way of moderating the solvent vapor concentration inside the chamber and hence the degree of swelling of the film. Solvent mixtures were injected into the annealing chamber through a Teflon capillary tube, whereas the nitrogen counter flow was used to help guide the evaporation rate of the solvents and control the thickness of the polymer film. Rapid drying of the film was achieved by opening the annealing chamber, which results in a rapid evaporation of the solvent, as observed visually by a change in the optical appearance of the film and in the film thickness as indicated by the Filmetrics spectroscopic reflectometer.

Characterization: Transmission electron microscopy (TEM) of the thermally annealed polymer was performed by sectioning ultra thin sections cut at −55 °C using a Leica Ultracut UCT microtome. The sections were transferred to copper grids and stained with phosphotungstic acid. Bright field TEM was performed on a FEI Tecnai G2 F20 TEM STEM operating at 120 kV. Atomic force microscopy (AFM) was performed on a Veeco Dimension 3100 Ambient AFM STM in tapping mode and used to observe the topography of the samples. Small-angle X-ray scattering (SAXS) data were collected at the Cornell High Energy Synchrotron Source beamline G1 with a multilayer monochromator ($\lambda = 1.457$ Å) with a 2D area detector and a sample-to-detector distance of 1.61 m. Data are presented as 1D plots of radially integrated intensity versus scattering vector q where $q = 4\pi\sin(\theta)\lambda^{-1}$, where 2θ is the total scattering angle. Grazing incidence small-angle X-ray scattering (GISAXS) experiments were conducted at beamline G1 as well. The station at G1 is equipped with a high-flux X-ray beam ($\approx 10^{13}$ photons/(s mm^2)) from a 50-pole wiggler in combination with a multilayer monochromator and harmonics rejection mirrors. A 2D Quantum 1 CCD detector was used to capture the scattered images at a beam energy of 9.8–10 keV. All images were taken at incident angle (α_i) that varied from 0.10° to 0.30°, which is both below and above the critical angle (α_{cp}) of the polymer film. GISAXS images were taken at periodic increments of time to probe any changes occurring within the film during solvent annealing. The film was moved slightly through the beam for each new exposure because it was found that exposure of the film to the beam cross-linked the polymer film and locked-in the morphology in the exposed spot.[6,11,15] In situ film thickness of the films was measured during the GISAXS scans. The spot on the film probed by the light beam for film thickness measurements was not exposed to X-ray beams.

Supporting Information

Supporting Information is available from the Wiley Online Library or from the author.

Acknowledgements

This work was supported by the National Science Foundation (NSF), DMR-1105253 and DMR-1409105. M.A.C. was supported by fellowships from the Alfred P. Sloan Foundation, IGERT-064112 Flexible Electronics for Life Science Applications, and the Coleman Family Foundation. Work was performed using facilities at the Cornell High Energy Synchrotron Source (CHESS); CHESS is supported by the National Science Foundation and the National Institute of Health/National Institute of General Medical Sciences under the NSF Award DMR-0936384 and the Cornell Center for Materials Research (CCMR; CCMR is supported by NSF award DMR 1120296, part of the NSF MRSEC program). The authors are grateful to Dr. Richard Vaia and Dr. Lawrence Drummy, Air Force Research Lab (AFRL), for their helpful discussion, Dr. Arthur Woll (CHESS) for his support at G1 and Dr. Marvin Paik (Cornell) for his initial help.

Received: November 16, 2014
Revised: March 12, 2015
Published online: April 11, 2015

[1] F. S. Bates, G. H. Fredrickson, *Annu. Rev. Phys. Chem.* **1990**, *41*, 525.
[2] a) M. Park, C. Harrison, P. M. Chaikin, R. A. Register, D. H. Adamson, *Science* **1997**, *276*, 1401; b) R. A. Segalman, *Science* **2008**, *321*, 919; c) T. Thurn-Albrecht, J. DeRouchey, T. P. Russell, H. M. Jaeger, *Macromolecules* **2000**, *33*, 3250.
[3] F. S. Bates, G. H. Fredrickson, *Phys. Today* **1999**, *52*, 32.
[4] E. W. Cochran, C. J. Garcia-Cervera, G. H. Fredrickson, *Macromolecules* **2006**, *39*, 2449.
[5] E. J. W. Crossland, M. Kamperman, M. Nedelcu, C. Ducati, U. Wiesner, D. M. Smilgies, G. E. S. Toombes, M. A. Hillmyer, S. Ludwigs, U. Steiner, H. J. Snaith, *Nano Lett.* **2008**, *9*, 2807.
[6] M. Y. Paik, J. K. Bosworth, D.-M. Smilges, E. L. Schwartz, X. Andre, C. K. Ober, *Macromolecules***2010**, *43*, 4253.
[7] a) S. H. Kim, M. J. Misner, T. P. Russell, *Adv. Mater.* **2004**, *16*, 2119; b) X. Gu, Z. Liu, I. Gunkel, S. T. Chourou, S. W. Hong, D. L. Olynick, T. P. Russell, *Adv. Mater.* **2012**, *24*, 5688; c) J. E. Seppala, R. L. Lewis, T. H. Epps, *ACS Nano* **2012**, *6*, 9855; d) P. Padmanabhan, M. Chavis, C. K. Ober, F. A. Escobedo, *Soft Matter* **2014**, *10*, 6172; e) W. I. Park, J. M. Kim, J. W. Jeong, Y. S. Jung, *ACS Nano* **2014**, *8*, 10009; f) M.-S. She, T.-Y. Lo, H.-Y. Hsueh, R.-M. Ho, *NPG Asia Mater.* **2013**, *5*, e42.
[8] S. H. Kim, M. J. Misner, L. Yang, O. Gang, B. M. Ocko, T. P. Russell, *Macromolecules* **2006**, *39*, 8473.
[9] K. Fukunaga, H. Elbs, R. Magerle, G. Krausch, *Macromolecules* **2000**, *33*, 947.
[10] C. Sinturel, M. n. Vayer, M. Morris, M. A. Hillmyer, *Macromolecules* **2013**, *46*, 5399.
[11] J. Bosworth, M. Paik, R. Ruiz, E. Schwartz, J. Huang, A. Ko, D. M. Smilgies, C. T. Black, C. K. Ober, *ACS Nano* **2008**, *2*, 1396.
[12] K. W. Gotrik, A. F. Hannon, J. G. Son, B. Keller, A. Alexander-Katz, C. A. Ross, *ACS Nano* **2012**, *6*, 8052.
[13] X. Gu, I. Gunkel, A. Hexemer, W. Gu, T. P. Russell, *Adv. Mater.* **2013**, *26*, 273.

[14] a) J. Y. Kelly, J. N. L. Albert, J. A. Howarter, C. M. Stafford, T. H. Epps, M. J. Fasolka, *J. Polym. Sci. Part B: Polym. Phys.* **2012**, *50*, 263; b) S. P. Paradiso, K. T. Delaney, C. J. Garcia-Cervera, H. D. Ceniceros, G. H. Fredrickson, *ACS Macro Lett.* **2014**, *3*, 16; c) J. N. L. Albert, W.-S. Young, R. L. Lewis, T. D. Bogart, J. R. Smith, T. H. Epps, *ACS Nano* **2012**, *6*, 459.
[15] J. Bosworth, C. T. Black, C. K. Ober, *ACS Nano* **2009**, *3*, 1761.
[16] J. G. Son, J.-B. Chang, K. K. Berggren, C. A. Ross, **2011**, *Nano Lett.11*, 5079.
[17] J. W. Jeong, W. I. Park, M.-J. Kim, C. A. Ross, Y. S. Jung, *Nano Lett.* **2011**, *11*, 4095.
[18] W. Bai, A. F. Hannon, K. W. Gotrik, H. K. Choi, K. Aissou, G. Liontos, K. Ntetsikas, A. Alexander-Katz, A. Avgeropoulos, C. A. Ross, *Macromolecules* **2014**, *47*, 6000.
[19] M.-S. She, T.-Y. Lo, R.-M. Ho, *Macromolecules* **2014**, *47*, 175.
[20] C. M. Papadakis, Z. Di, D. Posselt, D.-M. Smilgies, *Langmuir* **2008**, *24*, 13815.
[21] a) D. M. Smilgies, P. Busch, C. M. Papadakis, D. Posselt, *Synchrotron Radiat. News* **2002**, *15*, 35; b) S. H. Kim, M. J. Misner, T. Xu, M. Kimura, T. P. Russell, *Adv. Mater.* **2004**, *16*, 226; c) P. Du, M. Li, K. Douki, X. Li, C. B. W. Garcia, A. Jain, D. M. Smilgies, L. J. Fetters, S. M. Gruner, U. Wiesner, C. K. Ober, *Adv. Mater.* **2004**, *16*, 953.
[22] D. Yin, S. Horiuchi, T. Masuoka, *Chem. Mater.* **2005**, *17*, 463.
[23] J. Brandrup, E. H. Immergut, E. A. Grulke, A. Abe, D. R. Bloch, *Polymer Handbook*, 4th ed. Wiley, New York **2003**.
[24] L. Leibler, *Macromolecules* **1980**, *13*, 1602.
[25] D. W. Green, R. H. Perry, in *Chemical Engineering Handbook*, McGraw-Hill, New York **1934**.
[26] a) T. Harada, F. S. Bates, T. P. Lodge, *Macromolecules* **2003**, *36*, 5440; b) T. P. Lodge, B. Pudil, K. J. Hanley, *Macromolecules* **2002**, *35*, 4707.
[27] G. Krausch, R. Magerle, *Adv. Mater.* **2002**, *14*, 1579.
[28] a) K. A. Cavicchi, K. J. Berthiaume, T. P. Russell, *Polymer* **2005**, *46*, 11635; b) J. Peng, D. H. Kim, W. Knoll, Y. Xuan, B. Li, Y. Han, *J. Chem. Phys.* **2006**, 125.
[29] G. Kim, M. Libera, *Macromolecules* **1998**, *31*, 2569.
[30] a) Z. Di, D. Posselt, D.-M. Smilgies, C. M. Papadakis, *Macromolecules* **2010**, *43*, 418; b) J. Zhang, D. Posselt, D.-M. Smilgies, J. Perlich, K. Kyriakos, S. Jaksch, C. M. Papadakis, *Macromolecules* **2014**, *47*, 5711.
[31] I. Park, B. Lee, J. Ryu, K. Im, J. Yoon, T. Chang, M. Ree, *Macromolecules* **2005**, *38*, 10532.
[32] M. Q. Li, C. K. Ober, *Mater. Today* **2006**, *9*, 30.
[33] a) H. Mori, Wakisaka, A. Hirao, S. Nakahama, *Macromol. Chem. Phys.* **1994**, *195*, 3213; b) A. Hirao, H. Kato, K. Yamaguchi, S. Nakahama, *Macromolecules* **1986**, *19*, 1294; c) A. Boeker, A. H. E. Muller, G. Krausch, *Macromolecules* **2001**, *34*, 7477.